Materials Science Forum Vols. 790-791 (2014) pp 121-126

doi:10.4028/www.scientific.net/MSF.790-791.121

Influence of dendritic morphology on the calculation of macrosegregation in steel ingot

J. Li[1,2,3,a], M. Wu[1,2,b], A. Ludwig[2,c], A. Kharicha[1,2,d], P. Schumacher[4,e]

[1]Christian Doppler Lab for Adv. Process Simulation of Solidification and Melting,

[2] Chair of Simulation and Modeling of Metall. Processes, Univ. Leoben, 8700 Leoben, Austria

[3]School of Materials Science and Engineering, Shanghai Jiao Tong Univ., 200030 Shanghai, China

[4] Chair for Casting Research, University of Leoben, Austria

[a] li.jun@sjtu.edu.cn, [b] menghuai.wu@unileoben.ac.at, [c] ludwig@unileoben.ac.at,

[d] abdellah.kharicha@unileoben.ac.at, [e] peter.schumacher@unileoben.ac.at

Keywords: macrosegregation, steel ingot, solidification, modeling, A-segregation, columnar-to-equiaxed transition.

Abstract. The simulation of macrosegregation in a 2.45-ton steel ingot with the three-phase mixed columnar-equiaxed model was presented previously. The results showed an overestimation of the intensity of bottom negative segregation. The reason is due to the assumed globular morphology for the equiaxed crystal. Therefore, in this paper a simple approach is suggested to treat the dendritic morphology of equiaxed crystals. Three aspects are improved: the drag force between the moving equiaxed crystals and the surrounding melt, the mechanism of the columnar-to-equiaxed transition, the packing limit of the equiaxed crystals. The modified model is used to calculate the macrosegregation of the same ingot. It is found that the modified model predicts less severe negative segregation in the bottom equiaxed zone than the previous globular equiaxed model does, i.e. it agrees better to the experiment. The model considering simplified-dendritic morphology improves the calculation accuracy.

Introduction

On the solidification of ingot, the solutes are often redistributed non-uniformly in the fully solidified casting, giving birth to the segregation. Segregation occurring between and within dendritic arms is known as microsegregation. Macrosegregation refers to chemical variations over length scales approaching the dimensions of the casting, which for large ingots may be of the order of centimeters or even meters. Macrosegregation occurs in large steel ingots intensively. Therefore it is very important to understand its formation mechanism.

Since the experiment investigation in large steel ingot is very expensive, only very few experimental studies were found in literature since 1990s [1-2]. More and more people pay attention to the modeling study of steel ingot [3-7]. Gu and Beckermann [3] simulated the solidification of a 43-ton steel ingot. Their model was a single and the solid phase was assumed to be fixed. The predicted result of the vertical centerline segregation was in good agreement with the measured experimental values in the bottom and top regions. However, the neglect of the sedimentation of equiaxed crystals in the model leaded to the underestimation of the measured negative macrosegregation over the middle half of the ingot. Moreover, this model fails to predict A-segregation. Vannier and coworkers [4] presented a two phase model to study the macrosegregation of a 6.2 ton large steel ingot. The model was able to consider the heat, mass and momentum coupled transports during solidification of multicomponent alloys. The grain motion was still ignored. Combeau et al. [5-7] extended this model by considering the motion of equiaxed grains and also the evolution of grain morphology during solidification. However, these models did not take into account a realistic growth of the columnar phase. They just simply presumed a preinstalled columnar phase layer.

On the base of Wu and Ludwig's three-phase mixed columnar-equiaxed model [8-9], we calculated the macrosegregation in a 2.45-ton steel ingot [10-11]. Qualitatively, simulations agreed with experiments, but due to the assumption of globular morphology for the equiaxed crystals, the results showed an overestimation of the intensity of bottom negative segregation as well. In order to improve the modeling accuracy, in this paper the mixed columnar-equiaxed model (non-dendritic model) was modified by considering the dendritic morphology for equiaxed crystals. A simple approach was used to avoid the excessive increase of the calculation cost.

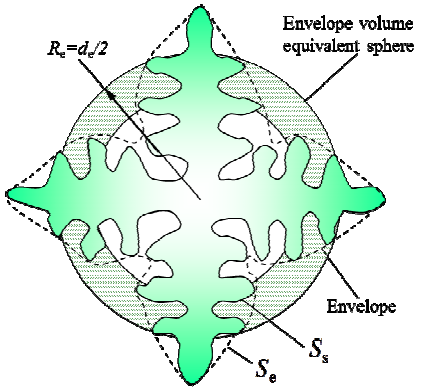

Fig.1 Schematic of the equiaxed dendritic structure and envelope.

Modeling Concept

As the assumption of globular equiaxed crystals leads to the significant deviation of the simulation result in the bottom equiaxed zone from the experimental result. Therefore, some modifications should be made in order to take into account the influence of equiaxed dendritic morphology. On the other hand, since the calculation of large steel ingot is exhausting, the improved model should not increase the calculation time so much. It is not a computationally efficient to embed the full dendritic model [12-13] into this model. Therefore, some simplifications are made to compromise the two aspects mentioned above. Here only the dendritic morphology of equiaxed crystal is considered.

An equiaxed dendrite is schematically shown in Fig. 1. Some important features are depicted as follows [13]:

1) The equiaxed dendrite envelope is defined as a smooth surface connecting the primary and secondary arm tips and contains both the solid dendrite and the interdendritic liquid. There are four phases in a control volume: the solid dendrites in the equiaxed grain, the interdendritic melt in the equiaxed grain, the extradendritic melt, and the columnar. The corresponding phase fractions are f_s^e, f_d^e, f_ℓ, and f_c with $f_\ell + f_d^e + f_s^e + f_c = 1$. For globular equiaxed crystals, f_d^e=0;

2) The volume fraction of equiaxed envelope includes two phase regions, $f_e = f_s^e + f_d^e$. The internal solid fraction within the envelope is calculated as $f_{si} = f_s^e / f_e$;

3) The interfacial area concentration, S_s and S_e, denoting the surface areas of the solid/interdendritic liquid and the surface area of the dendrite envelope, respectively, divided by the volume of the control element.

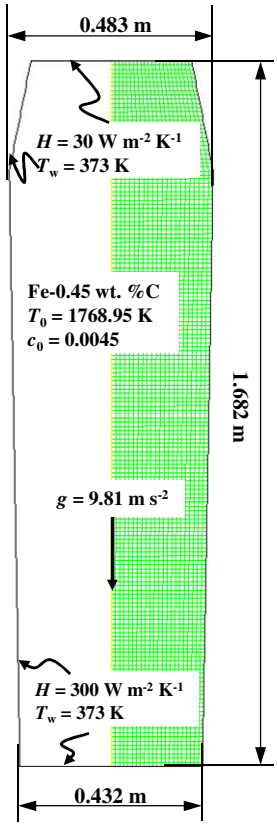

Fig. 2 Configuration of 2.45-ton steel ingot

As discussed above, the motivation of developing this model is to take into account the equiaxed dendritic structure without increasing the calculation time. Therefore, one simplification is made here: the internal solid fraction within the equiaxed envelope, f_{si}, was assumed to begin with a constant value of f_{si}^c. When the volume fraction of solid dendrites, f_s^e, is bigger than f_{si}^c, f_{si} is assumed to be equal to f_s^e. Here f_{si}^c must be determined experimentally or assumed empirically. With the above assumption all the parameters required can be derived based on the previous three-phase mixed columnar-equiaxed model [13].

The model is the same as the non-dendritic model [8-11, 14-15]. Three parts are modified when considering the simplified equiaxed dendritic morphology:

1) The drag force between the equiaxed and liquid phases is calculated according to a multiparticle interfacial drag force law [16];

2) The critical volume fraction of equiaxed crystals to block the growth of the primary columnar dendrite tips (CET mecahnism), is set as $0.49 \cdot f_{si}$, instead of 0.49 in the previous model [10-11].
3) The packing limit ($f_{e,pack}$ =0.637) of equiaxed crystals is modified accordingly, $f_{e,pack} = 0.637 / f_{si}$.

Configuration of the Ingot

A 2.45-ton big-end-up steel ingot (Fe-0.45 wt.% C) is simulated [17]. The ingot had a square, cross-sectional area and was cast in a chilled mould; here a 2-D axis-symmetrical simulation was performed to approximate the solidification behavior in the square cross-section of the ingot. The configuration of this ingot, labeled with the necessary boundary and initial conditions, is described in Fig. 2. All the thermodynamic and physical properties used in this study are the same as reference [12], as shown in Table 1. Because the experiment was performed many decades ago and because of the lack of a precise process description, assumptions must be made for certain process parameters and boundary conditions. Here, the heat transfer coefficient is based on the final solidification time, which refers to the classical theory and experimental values [18].

Table 1. Thermodynamic & physical properties

Property	Symbols	Units	Quantity
Melting of pure iron	T_f	K	1805.15
Liquidus slope	m	K (wt.%)$^{-1}$	-80.45
Equilibrium partition coefficient	k	-	0.36
Reference density	ρ_ℓ, ρ_e, ρ_c	kg·m^3	6990
Solid-liquid density difference	$\Delta\rho$	kg·m^3	150
Specific heat	c_p^ℓ, c_p^c, c_p^e	J·kg^{-1}·K^{-1}	500
Thermal conductivity	k_ℓ, k_e, k_c	W·m^{-1}·K^{-1}	34.0
Latent heat	L	J·kg^{-1}	2.71×10^5
Viscosity	μ	Kg·m^{-1}·s^{-1}	4.2×10^{-3}
Thermal expansion coefficient	β_T	K^{-1}	1.07×10^{-4}
Solutal expansion coefficient	β_c	wt.%$^{-1}$	1.4×10^{-2}
Dendritic arm spacing	λ_1	m	5×10^{-4}
Diffusion coefficient (liquid)	D_ℓ	m^2·s^{-1}	2.0×10^{-8}
Diffusion coefficient (solid)	D_e, D_c	m^2·s^{-1}	1.0×10^{-9}

Result and Discussion

The solidification sequence and segregation index were compared between non-dendritic and simplified-dendritic models, as shown in Fig. 3. As we can see, the general solidification sequences between these two models are the same, including: the stationary columnar dendrites grow from the mold wall, and the columnar tip front moves inwards; the sedimentary equiaxed grains nucleate near the mold walls, sink and settle at the base of the ingot which results in a characteristic conic shape. More equiaxed grains are found in the lower region of the ingot, whereas columnar structures are found predominant in the upper region of the ingot. The flow in the ingot is driven by three forces: the solutal buoyancy force, which leads to upward flow; the thermal buoyancy force, which leads to downward melt flow; and the motion of the sinking equiaxed crystals, which drags the surrounding melt downwards. Initially, the two downward forces are dominant along the side walls of the ingot. The downward flow and the sinking equiaxed crystals change direction at the bottom of the ingot, move inwards, and then rise in the middle region of the ingot. Meanwhile, the cooled melt at the casting top tends to sink directly from the middle part of the ingot. The upward and downward flows interact with each other, and the resulting global flow pattern is highly unstable and disordered. Large eddies develop dynamically and then are suppressed in the bulk region.

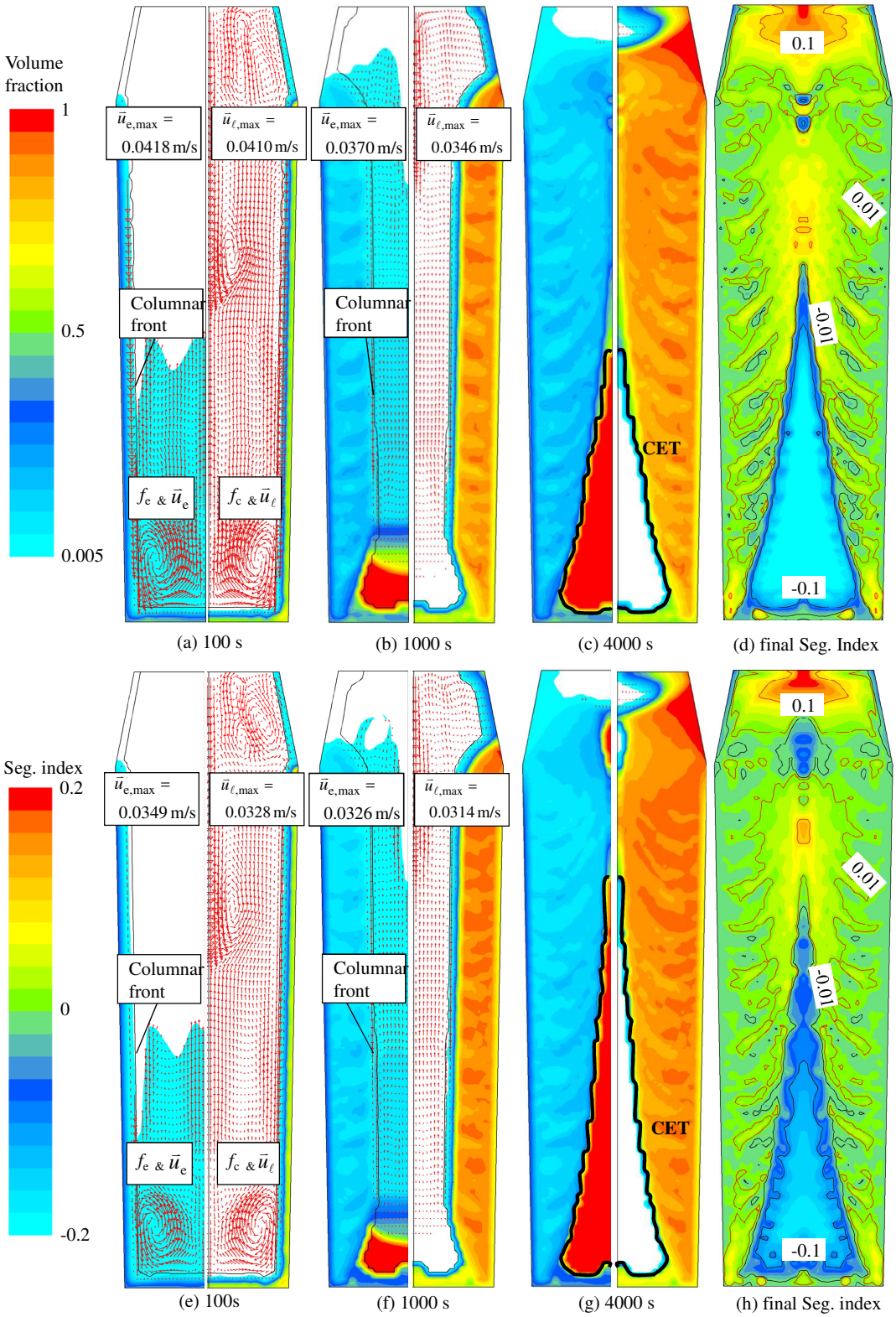

Fig. 3 Predicted solidification sequence and formation of macrosegregation. The upper raw shows the results of non-dendritic model, while the low raw shows the results of simplified-dendritic model. For (a)-(c) and (e)-(g), in the left half the equiaxed volume fraction is overlapped with the equiaxed velocity, in the right half the columnar volume fraction is overlapped with liquid velocity. (d) and (h) shows the final segregation index ($(c_{mix} - c_0)/c_0$) overlapped with some iso-values.

When the equiaxed dendritic structure is considered the drag force between sinking equiaxed crystal and surrounding melt becomes larger by comparison with the case of non-dendritic model. Thus the equiaxed sinking speed is decreased and subsequently the liquid velocity is also decreased, as we see from Fig. 3(a)-(b) and (e)-(f). At 100 s the non-dendritic model predicts the maximum equiaxed and liquid velocity of 0.0418 m/s and 0.0410 m/s, whereas the simplified-dendritic model predicts 0.039 m/s and 0.0328 m/s, correspondingly. In addition, the columnar-to-equiaxed-transition (CET) zone for the simplified-dendritic model is prolonged, as shown in Fig. 3(c) and (g). The final macrosegregation patterns (Fig. 3 (e) and (h)) predicted by both non-dendritic and simplified-dendritic models are similar: the positive segregation zone in the top part, the cone shape negative segregation zone in the bottom region, and many quasi A-segregation bands. The distribution of these quasi A-segregation bands is also similar for these two cases. For simplified-dendritic equiaxed case, the cone shape negative segregation region has been prolonged.

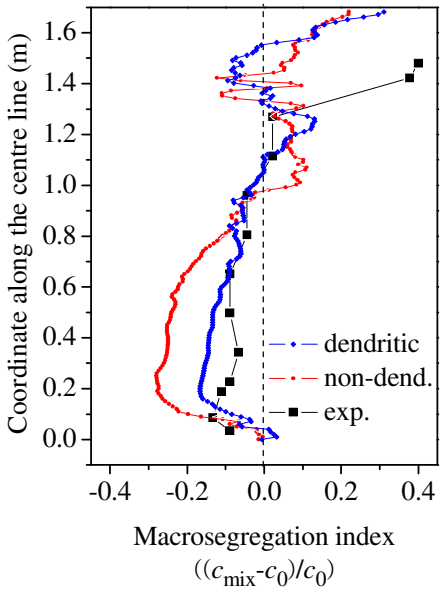

Fig. 4 Comparison of centerline macrosegregation.

Fig. 4 presents the centerline macrosegregation of non-dendritic model, simplified dendritic model and experiment [17]. The general distribution of centerline segregation is the same for non-dendritic case and simplified-dendritic case. However, it is obvious that the simplified dendritic equiaxed model predicted less serious negative segregation in the bottom region than the non-dendritic model. The simplified-dendritic model predicts a very nice agreement with the experiment result in the bottom region. It demonstrates that the simplified dendritic model improves the accuracy of the calculation significantly.

Summary

The three-phase mixed columnar-equiaxed solidification model [8-9] was modified to consider the dendritic morphology of equiaxed crystals. This was used to calculate the macrosegregation in a 2.45-ton steel ingot. By comparison with the non-dendritic model, the simplified-dendritic model predicted: smaller equiaxed and liquid velocity; more extended CET zone; the same macrosegregation pattern; less severe negative segregation in the bottom equiaxed zone. The predicted centreline segregation by the simplified dendritic model was more close to the experiment result than the non-dendritic model did. The simplified dendritic model improved the calculation accuracy for the macrosegregation significantly.

Acknowledgments

The authors are grateful for financial support from the Austrian Federal Ministry of Economy, Family and Youth, from the National Foundation for Research, Technology and Development within the framework of the Christian-Doppler Laboratory for Advanced Process Simulation of Solidification and Melting, and from the FWF Austrian Science Fund (P23155-N24). Jun Li would like to thank the China Scholarship Council for their generous support.

References

[1] J. Wang, P. Fu, H. Liu, D. Li, Y. Li, Shrinkage porosity criteria and optimized design of a 100-ton 30Cr2Ni4MoV forging ingot, Mater. Design 35 (2012) 446-456.

[2] P. Machovčák, A. Opler, Z. Carbol, A. Trefil, K. Merta, J. Zaoral, M. Tkadlečková, K. Michalek, Evaluation of chemical heterogeneity of a 90-ton forging ingot, Archives of Mater. Sci. Eng. 58 (2012) 22-27.

[3] J. P. Gu, C. Beckermann, Simulation of convection and macrosegregation in a large steel ingo, Metall. Mater. Trans. A 30 (1999) 1357-1366.

[4] I. Vannier, H. Combeau, G. Lesoult, Numerical model for prediction of the final segregation pattern of bearing steel ingot, Mater. Sci. Eng. 173A (1993) 317-321.

[5] H. Combeau, A. Kumar, M. Zalonik, Modeling of equiaxed grain evolution and macrosegregations development in steel ingots, Transactions Indian Institute of Metals 62 (2009) 285-290.

[6] H. Combeau, M. Zaloznik, S. Hans, P. Richy, Prediction of macrosegregation in steel ingot: influence of the motion and the morphology of equiaxed grains, Metall. Mater. Trans. B 40B (2009) 289-304.

[7] A. Kumar, M. Zaloznik, and H. Combeau, Prediction of equiaxed grain structure and macrosegregation in an industrial steel ingot: comparison with experiment, Int. J. Adv. Eng. Sci. Appl. Math. 2 (2010) 140-148.

[8] M. Wu, A. Ludwig, A three-phase model for mixed columnar equiaxed solidification, Metall. Mater. Trans. A 37A (2006) 1613-1631.

[9] M. Wu, A. Ludwig, Using a three-phase deterministic model for the columnar-to-equiaxed transition, Metall. Mater. Trans. A 38A (2007) 1465-1475.

[10] J. Li, M. Wu, A. Ludwig, A. Kharicha, Modelling macrosegregation in a 2.45 ton steel ingot, in: A. Ludwig, M. Wu, A. Kharicha (Eds.), MCWASP XIII, Schladming, Austria, 2012, IOP Conf. Series: Mater. Sci. Eng. 33 (2012) 012091.

[11] J. Li, M. Wu, A. Ludwig, A. Kharicha, Simulation of macrosegregation in a 2.45-ton steel ingot using a three-phase mixed columnar-equiaxed model, Int. J. Heat Mass Transfer (2013) doi : 10.1016/j.ijheatmasstransfer.2013.08.079

[12] M. Wu, A. Ludwig, Modeling equiaxed solidification with melt convection and grain sedimentation-I: Model description, Acta Materialia, 57 (2009) 5621-5631.

[13] M. Wu, A. Fjeld, A. Ludwig, Modelling mixed columnar-equiaxed solidification with melt convection and grain sedimentation-Part I: Model description, Comp. Mater. Sci., 50 (2010) 32-42.

[14] J. Li, M. Wu, J. Hao, A. Ludwig, Simulation of channel segregation using a two-phase columnar solidification model – Part I: Model description and verification, Comp. Mater. Sci., 55 (2012) 407-418.

[15] J. Li, M. Wu, J. Hao, A. Ludwig, Simulation of channel segregation using a two-phase columnar solidification model – Part II: Mechanism and parameter study, Comp. Mater. Sci., 55 (2012) 419-429.

[16] C. Wang, S. Ahuja, C. Beckermann, H. Groh, Multi- particle interfacial drag in equiaxed solidification, Metall. Mater. Trans. B, 26B (1995) 111-119.

[17] Report on the heterogeneity of steel ingots, J. Iron Steel Inst. 113 (1926) 39-176.

[18] E. Marburg, Accelerated solidification in ingot: its influence on ingot soundness, Journal of Metals, 5 (1953) 157-172.